Spin-Polarized Surface State in EuO(100)

Jürgen Klinkhammer,[1] Martin Schlipf,[2] Fabian Craes,[1] Sven Runte,[1] Thomas Michely,[1] and Carsten Busse[1,*]
[1]*II. Physikalisches Institut, Universität zu Köln, Zülpicher Straße 77, 50937 Köln, Germany*
[2]*Peter Grünberg Institut, Forschungszentrum Jülich and JARA, 52425 Jülich, Germany*
(Received 13 May 2013; revised manuscript received 24 October 2013; published 7 January 2014)

High-quality films of the ferromagnetic semiconductor EuO are grown on epitaxial graphene on Ir(111) and investigated *in situ* with scanning tunneling microscopy and spectroscopy. Electron scattering at defects leads to standing-wave patterns, manifesting the existence of a surface state in EuO. The surface state is analyzed at different temperatures and energies. We observe a pronounced energy shift of the surface state when cooling down below the Curie temperature T_C, which indicates a spin polarization of this state at low temperatures. The experimental results are in agreement with corresponding density functional theory calculations.

DOI: 10.1103/PhysRevLett.112.016803 PACS numbers: 73.20.At, 68.37.Ef, 68.47.Fg, 68.47.Gh

Spin-polarized surface states are the key ingredient for the special behavior of three-dimensional topological insulators [1], for example in Bi_2Se_3 [2]. This also leads to a renewed interest in spin-polarized surface states of topologically trivial materials. A classical example are the Rashba-split states found on metals with large nuclear charge like Au(111) [3] or Bi(111) [4], and the exchange-split states on magnetic materials like Ni(111) [5]. Of specific interest are spin-polarized surface states intersecting the Fermi level as they contribute significantly to charge transport [2].

For the ferromagnetic semiconductor europium oxide (EuO) [6], an exchange-split surface state below the conduction band was predicted more than ten years ago by Schiller and Nolting [7] in ferromagnetic Kondo lattice model calculations. It withstood experimental observation until now [8], because it is completely in the unoccupied part of the band structure which is harder to address experimentally. The surface state is pinned to the conduction band, and in consequence both are spin split in the ferromagnetic state (bulk Curie temperature $T_C = 69$ K [6]). The spin splitting of the surface state is calculated to be $\Delta E = 0.78$ eV. The bottom of the conduction band becomes completely spin polarized [9]. It is also speculated that for $T \to 0$ the low-energy spin-up state moves below the Fermi energy E_F, making the surface half-metallic [7]. A practical interest in EuO arises in the field of spintronics, where thin films are used as a spin filter material that shows a high degree of spin polarization [10]. For thin films like this, the electronic properties of the surface can play a significant role. Here, we report the first experimental observation of the spin-split surface state in EuO, complemented by dedicated results from density functional theory (DFT).

Sample preparation and analysis are performed in a low-temperature ultrahigh vacuum system which consists of a preparation chamber with a base pressure of $p = 1.0 \times 10^{-10}$ mbar and a scanning tunneling microscopy (STM) chamber with a He bath cryostat ($p < 7 \times 10^{-11}$ mbar). Substrate cleaning, graphene preparation, and the growth of EuO is monitored using low energy electron diffraction (LEED). Thin films of 3.3 nm are grown on graphene on Ir(111) by reactive molecular beam epitaxy with Eu surplus at $T = 300$ K, followed by annealing in an Eu atmosphere. This leads to stoichiometric EuO films (supported by Eu-intercalated graphene) with a perfect [100] out-of-plane texture and random in-plane orientation that show a slightly enhanced $T_C \approx 75$ K [11]. The structure of the graphene layer itself is not changed in this preparation [11,12]. The samples are transferred into the cryostat, where they stay clean for weeks and are analyzed with STM and scanning tunneling spectroscopy (STS) using a high-stability beetle-type STM with etched W-tips. The tip is virtually grounded and the sample is put to the bias voltage U leading to a tunneling current I. Energies are connected to U by $E - E_F = eU$. The differential conductivity dI/dU [representing the local density of states (LDOS)] is measured by lock-in technique, adding a harmonic modulation of 12 mV at 883.7 Hz to U. We measure both at the base temperature of the STM of 5.3 K as well as at elevated temperatures, heating the STM by a reverse-biased diode. The piezo actuators of the STM are calibrated using atomically resolved topography images of EuO, with the Eu next-nearest-neighbor distance determined by LEED [11]. STM images are processed using WSxM [13].

Our experiments are complemented by DFT calculations [14,15] within the GGA + U approach. The surface of the finite thickness EuO(100) film is modeled neglecting the substrate. Keeping the in-plane lattice constant fixed to the experimental value, we relax the positions of all the atoms along the out-of-plane direction with the projector augmented-wave method [16,17] using a supercell approach. In order to minimize the interaction between the two surfaces of adjacent unit cells, we calculate a film of 15 layers in a supercell separated by 10.3 Å of vacuum. With these relaxed positions, we perform a spin-polarized,

true two-dimensional calculation with an all-electron full-potential linearized-augmented-plane-wave scheme [18] using slab-approach with semi-infinite vacuum at both sides of the slab. We employ the PBE-GGA functional [19] and include an on-site Hubbard-like correction [20] to improve the description of the localized Eu $4f$ and O $2p$ states with parameters chosen according to Ref. [21]. The calculations describe the case of $T = 0$ K and thus $T < T_C$. For temperatures above T_C, the expected band structure is very well approximated by the average between the spin-up and the spin-down results.

The EuO(100) surface shows large, atomically flat terraces in STM, where we occasionally find shallow and extended apparent depressions [see Fig. 1(a)] that we attribute to oxygen vacancies (see below). The experimentally determined concentration of O vacancies is 0.3%, and thus more than an order of magnitude below the amount that causes a metal-to-insulator transition (MIT) [22]. In consequence, dI/dU point spectra show no LDOS at E_F even below T_C (not shown). Figure 1(b) shows a dI/dU map of the unoccupied LDOS measured in constant current mode at 1.25 eV and 5.3 K. Concentric rings are visible around the defect sites, and the scattering patterns of neighboring defects interfere with each other. This is a fingerprint for scattering processes of electrons in a surface state. The inset shows the Fourier transform (FT) of a Laplace-filtered large scale dI/dU map where a single ring typical for a free-electron-like surface state is visible [23]. The radius $k_{\mathrm{FT}}(E - E_F)$ of the ring is related to the wave vector k of the electrons by $2k(E - E_F) = k_{FT}(E - E_F)$ [23]. From the data shown in Fig. 1(b), we derive $k(1.25\ \mathrm{eV}) = 3.88\ \mathrm{nm}^{-1}$ for $T = 5.3$ K.

In a simplified analysis method, $k(E - E_{\mathrm{F}})$ is determined in real space by measuring the wavelength λ of the sinusoidal modulations of the LDOS patterns (see Fig. 2 for two examples at the same energy but different temperatures).

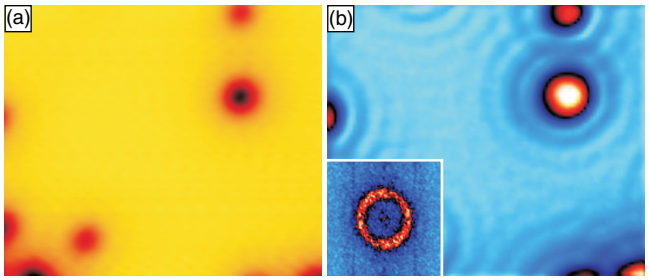

FIG. 1 (color online). (a) STM topography image of a closed EuO(100) film containing point defects, stabilization parameters: $U = 1.25$ V, $I = 0.77$ nA, scan size 10.3 nm × 8.8 nm, imaged at 5.3 K. (b) Simultaneously recorded differential conductivity dI/dU map (contrast is enhanced by adding the spatial derivative to the signal). Circular standing-wave patterns of electrons scattered at point defects are visible. Inset: Fourier transform (width 36.6 nm^{-1}) of a large-scale Laplace-filtered dI/dU map containing the area shown in (b).

The differential conductivity maps show standing-wave patterns of the surface state resulting from scattering at point and line defects. Normalized line profiles as marked by the red (gray) and black lines in Figs. 2(b) and 2(d) are used to measure λ. The distance between two minima amounts to $\lambda(1.50\mathrm{eV}) = (0.699 \pm 0.010)\,\mathrm{nm}$ for 5.3 K and $\lambda(1.50\mathrm{eV}) = (0.885 \pm 0.010)\,\mathrm{nm}$ for 81.0 K; i.e., the scattering patterns at high temperatures have a significantly larger periodicity. We relate λ to k via $\lambda = 2\pi/k_{\mathrm{FT}} = \pi/k$. We mostly rely on the real space evaluation method because it is especially suited to evaluate the scattering patterns at one-dimensional defects like step edges or grain boundaries. Overall, we performed STS measurements over a wide range of energies (−3.0 to 3.0 eV). The resulting dispersion relations $k(E - E_F)$ are shown as red (gray)

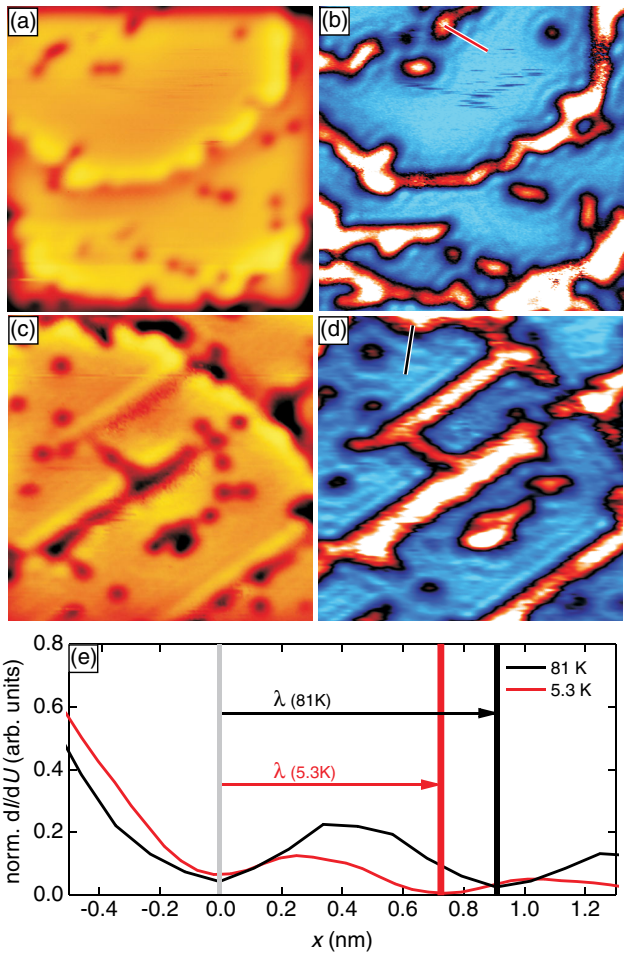

FIG. 2 (color online). (a) STM topography and (b) same area differential conductivity dI/dU map at 5.3 K measured on 3.3 nm EuO(100). Scattering is observed at step edges. Stabilization parameters: $U = 1.50$ V, $I = 0.073$ nA, scan width 16.5 nm. (c) STM topography and (d) same area dI/dU map of the same sample, but different area at 81.0 K. Scattering is observed at line defects. Stabilization parameters: $U = 1.50$ V, $I = 0.033$ nA, scan width 16.5 nm. (e) Line profiles of dI/dU as indicated by the red (gray) and black line in (b) and (d).

($T = 5.3$ K) and black data points ($T = 81.0$ K) in Fig. 3. The results from the FT and the real space method are in good agreement. The data at high temperatures are shifted upwards with respect to the low temperature ones by (0.32 ± 0.02) eV. The characteristic features of an unoccupied, electron-like surface state are evident, as predicted in Ref. [7]. Hence, our measurements are the first experimental proof for the existence of the surface state on EuO(100).

The band structure resulting from our DFT calculations qualitatively agrees with earlier work [7] (see the Supplemental Material [24] for the full picture). On close inspection, however, significant differences between our largely *ab initio* treatment and the earlier work based on model Hamiltonians become evident. In our case the parabolic spin-up surface state overlaps with the corresponding bulk band in the vicinity of the Γ point. Furthermore, ΔE is smaller than calculated before (0.37 eV), and the spin-up branch does not touch the Fermi energy, so that the predicted half metallic behavior [7] is absent.

As a first step, we compare the theoretical results for temperatures above T_C (spin-degenerate case) to our experiment. The shape of our experimental dispersion curve (black data points in Fig. 3) agrees with the one

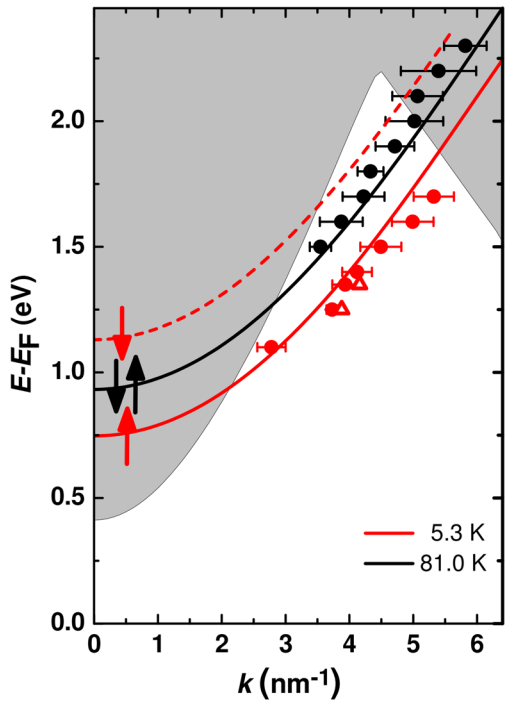

FIG. 3 (color online). Dispersion relation: $(E - E_F)$ vs wave vector k. Red (gray): Sample temperature 5.3 K. Black: Sample temperature 81.0 K. Full dots: Real-space method. Open triangles: Fourier transform method (see text). Lines and gray area: Results from density functional calculations (downshifted by 0.41 eV; see text). Lines: surface state, red (gray): 0 K, solid: spin up, dashed: spin down. Black: Spin averaged state $T > T_C$. Gray area: bulk band at 0 K, projected on the parallel momentum k. Note that the bulk band at $T > T_C$ is not at the same position.

of the surface state determined in our calculations as can bee seen when the calculated dispersion is downshifted by 0.41 eV (this downshift was fitted by taking both the high and low temperature data into account, see below). One reason for the downshift may be the uncertainty of the Hubbard U parameter employed on the $4f$ states in the calculation, which directly shifts the Fermi energy and hence the position of the surface state. Furthermore, the reduced screening as well as the band narrowing near the surface may alter the value of U [25]. In addition, there can also be experimental reasons for this shift: as the EuO work function of $\Phi_{\mathrm{EuO}} = (0.6 \pm 0.3)$ eV [26] is much lower than the one of Eu-intercalated graphene of $\Phi_{\mathrm{gr/Eu/Ir}} \approx 3$ eV [27], a charge transfer from EuO to its substrate seems feasible, which would cause an upshift of all EuO bands. Note, however, that this effect can only be weak as even a small shift would already push the Eu $4f$ levels above the Fermi level (see the Supplemental Material [24]). As we did not observe any change in the dispersion relation upon varying the tunneling resistance by a factor of four, we rule out tip-induced band bending [28,29].

For the case of low temperatures, our theoretical results predict the surface state to be fully spin split (dashed and/or solid red (gray) line in Fig. 3); i.e., it follows the bulk conduction band (see the Supplemental Material [24]). Using the same downshift as above, we find good agreement between our experimental dispersion relation [red (gray) data points in Fig. 3] and the spin-up branch found in theory. In consequence, the experimentally observed shift of the surface state to lower energies for the case of low temperature can be straightforwardly explained by the Stoner-like spin splitting.

Experimentally, we do not observe the corresponding spin-down branch (note that for an exchange-split surface state it is not fundamentally forbidden to observe the spin splitting in STM studies of standing-wave patterns, in contrast to Rashba-split states [30]). We propose that the spin-down state remains invisible as it largely overlaps with bulk bands (gray area in Fig. 3). Note that this overlap also explains the absence of scattering patterns for the spin-up state at low as well as high energies. Even though the lower edge of the bulk is formed by spin-up electrons, a spin-down surface state electron may decay into the bulk by undergoing spin-flip scattering which has a low, but finite probability. This only leaves a small window where the spin-down band could be observed in principle. However, in this regime we are already at high energies where tunneling conditions get unstable. Furthermore, the expected pattern with a long wavelength will be difficult to observe in the presence of the short-scale pattern of the spin-up state at the same E. Finally we note that in related studies also a spin dependence of the scattering mechanisms at defects was found [5], so that the observability of a scattering pattern for a given state at specific

defects is not *a priori* given. In view of the above, our experimental value for the spin splitting amounts to twice the splitting between the spin-up and the spin-degenerate branch, i.e. $\Delta E = (0.64 \pm 0.03)$ eV.

Finally, we analyze the atomic structure of the point scatterers observed in Fig. 1. In Fig. 4(a) we show the typical topography of a defect in EuO(100) around 1.50 V. A depression with a depth of 0.06 nm is imaged [see Fig. 4(c)]. As the depth is less than the height of one monolayer of EuO and the structure is rather smooth, we propose that electronic effects dominate over structural ones here. Atomic resolution imaging at −0.68 V of the same sample area shows an atomically flat and well ordered surface, as displayed in Fig. 4(b). Since the EuO band structure is dominated by Eu states around the Fermi level [31] one just images the Eu atoms and not the O atoms [11]. Clearly, the center of the depression [marked by a box in Fig. 4(a), which is duplicated at the same location in Fig. 4(b)], coincides with the lattice position of an O atom. As the samples are grown and annealed under excess of Eu, the existence of O vacancies is highly probable. In consequence, we assign the electronic defects observed here to oxygen vacancies. A statistical analysis of the apparent depths of the electronic defects measured under identical tunneling conditions reveals three pronounced levels [Fig. 4(d)]. We speculate that these differences are caused by the oxygen vacancies being located in different lattice planes, where the strongest electronic contrast is caused by a defect in the top layer. In consequence, the electronic defect in Fig. 4(a) is identified as an oxygen vacancy in the third layer below the surface. We observe no dependence of the definition of the scattering patterns on the depth of the oxygen vacancy, indicating that this kind of defect is always a sufficiently strong scatterer.

The electronic properties of the EuO in the vicinity of the defect sites can be addressed using the local apparent barrier height Φ which is related to the work function Φ_s (Φ_t) of the sample (tip) via $\Phi = 1/2(\Phi_t + \Phi_s - eU)$ [27]. Φ is determined by fitting an exponential decay to $I(z)$ spectra, where z is the vertical tip-to-sample distance. Figure 4(e) shows the local variation of Φ across two defect sites. The local work function Φ_s of the sample drops by 0.2 eV above an oxygen vacancy site [as indicated by the arrows in Fig. 4(e)]. Consequently, we propose that the defect is positively charged [32]. Formally removing an O^{2-}-ion from the lattice would result in such a positively charged defect, also denoted an F^{2+} color center. Such a defect can trap one (F^{+}) or two (F^{0}) electrons. Our finding of a reduction of the local work function indicates a color center of type F^{2+} or F^{+}. The local charge does not influence the dispersion relation of the surface state (Fig. 3), because we evaluated the scattering patterns in a sufficient distance (> 1.5 nm) away from the defect.

To conclude, we have investigated the electronic structure of EuO(100) via the analysis of scattering patterns of surface electrons. Thereby, we have experimentally verified the prediction of a spin-split surface state on stoichiometric EuO with ΔE as large as (0.64 ± 0.03) eV. Our experimental results agree with the calculated band structure. The proposed half-metallic behavior of the surface state is absent.

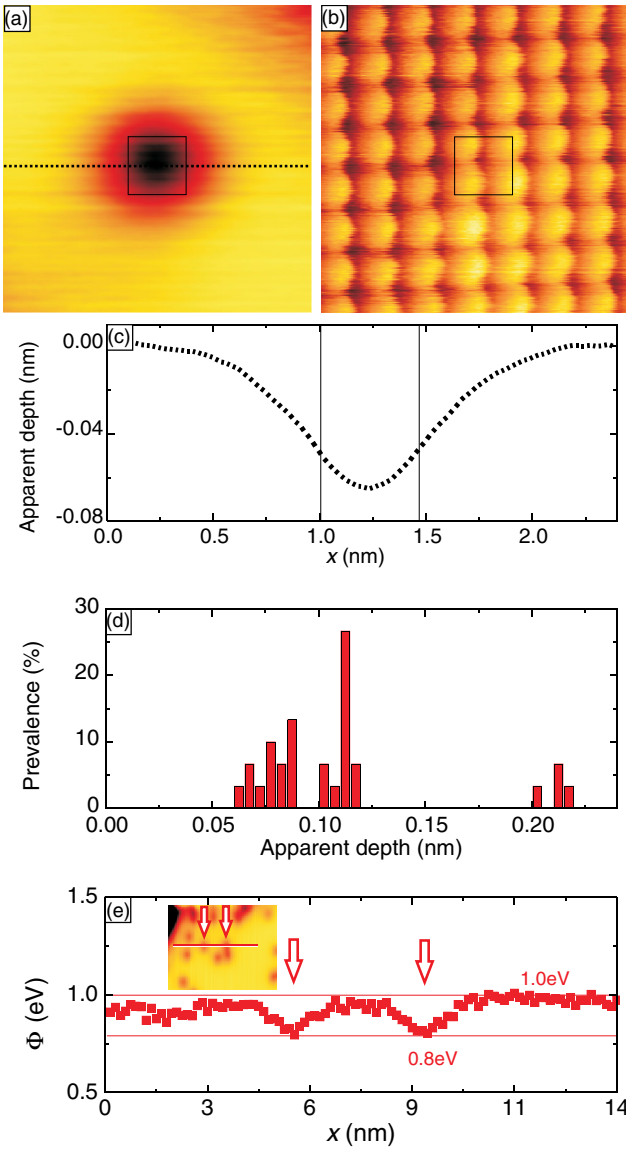

FIG. 4 (color online). (a) STM topography of EuO(100). Tunneling parameters: $U = 1.51$ V, $I = 0.15$ nA. (b) Atomically resolved STM topography image of the same sample area as in (a), imaged with $U = -0.68$ V, $I = 0.10$ nA, scan width 2.5 nm. The black box in (a) and (b) marks the same sample area. (c) Height profile along the horizontal line in (a). (d) Statistics of the maximum apparent depth of depressions measured under identical tunneling conditions as in (a). (e) The apparent barrier height Φ of the tunneling junction is determined by local $I(z)$) spectra measured along the red (gray) line in the inset, where z is the vertical tip-sample distance. Two defect sites are marked by arrows. Spectra parameter: Stabilization at $U_{stab} = 0.96$ V and $I_{stab} = 0.51$ nA, retraction to $U = 0.70$ V. Inset: STM topography of EuO(100), scan size 18.3 nm × 14.4 nm, $U = 0.95$ V, $I = 0.51$ nA, imaged at 5.3 K.

We acknowledge S. Schumacher for experimental help. The theory part benefitted from the support of S. Blügel and M. Ležaić. This work was funded by DFG through SFB 608 and INST 2156/514-1.

*busse@ph2.uni-koeln.de

[1] M. Z. Hasan and C. L. Kane, Rev. Mod. Phys. **82**, 3045 (2010).
[2] Y. Xia, D. Qian, D. Hsieh, L. Wray, A. Pal, H. Lin, A. Bansil, D. Grauer, Y. S. Hor, R. J. Cava, and M. Z. Hasan, Nat. Phys. **5**, 398 (2009).
[3] S. LaShell, B. A. McDougall, and E. Jensen, Phys. Rev. Lett. **77**, 3419 (1996).
[4] Y. M. Koroteev, G. Bihlmayer, J. E. Gayone, E. V. Chulkov, S. Blügel, P. M. Echenique, and P. Hofmann, Phys. Rev. Lett. **93**, 046403 (2004).
[5] K.-F. Braun and K.-H. Rieder, Phys. Rev. B **77**, 245429 (2008).
[6] B. T. Matthias, R. M. Bozorth, and J. H. Van Vleck, Phys. Rev. Lett. **7**, 160 (1961).
[7] R. Schiller and W. Nolting, Phys. Rev. Lett. **86**, 3847 (2001).
[8] D. E. Shai, A. J. Melville, J. W. Harter, E. J. Monkman, D. W. Shen, A. Schmehl, D. G. Schlom, and K. M. Shen, Phys. Rev. Lett. **108**, 267003 (2012).
[9] P. G. Steeneken, L. H. Tjeng, I. Elfimov, G. A. Sawatzky, G. Ghiringhelli, N. B. Brookes, and D.-J. Huang, Phys. Rev. Lett. **88**, 047201 (2002).
[10] T. S. Santos and J. S. Moodera, Phys. Rev. B **69**, 241203 (2004).
[11] J. Klinkhammer, D. F. Förster, S. Schumacher, H. P. Oepen, T. Michely, and C. Busse, Appl. Phys. Lett. **103**, 131601 (2013).
[12] R. Larciprete, S. Ulstrup, P. Lacovig, M. Dalmiglio, M. Bianchi, F. Mazzola, L. Hornekær, F. Orlando, A. Baraldi, P. Hofmann, and S. Lizzit, ACS Nano **6**, 9551 (2012).
[13] I. Horcas, R. Fernandez, J. M. Gomez-Rodriguez, J. Colchero, J. Gomez-Herrero, and A. M. Baro, Rev. Sci. Instrum. **78**, 013705 (2007).
[14] P. Hohenberg and W. Kohn, Phys. Rev. **136**, B864 (1964).
[15] W. Kohn and L. J. Sham, Phys. Rev. **140**, A1133 (1965).
[16] P. E. Blöchl, Phys. Rev. B **50**, 17953 (1994).
[17] G. Kresse and J. Furthmüller, Phys. Rev. B **54**, 11169 (1996).
[18] http://www.flapw.de.
[19] J. P. Perdew, K. Burke, and M. Ernzerhof, Phys. Rev. Lett. **77**, 3865 (1996).
[20] V. I. Anisimov, F. Aryasetiawan, and A. I. Lichtenstein, J. Phys. Condens. Matter **9**, 767 (1997).
[21] N. J. C. Ingle and I. S. Elfimov, Phys. Rev. B **77**, 121202 (2008).
[22] S. G. Altendorf, A. Efimenko, V. Oliana, H. Kierspel, A. D. Rata, and L. H. Tjeng, Phys. Rev. B **84**, 155442 (2011).
[23] L. Petersen, P. T. Sprunger, P. Hofmann, E. Lægsgaard, B. G. Briner, M. Doering, H. P. Rust, A. M. Bradshaw, F. Besenbacher, and E. W. Plummer, Phys. Rev. B **57**, R6858 (1998).
[24] See Supplemental Material at http://link.aps.org/supplemental/10.1103/PhysRevLett.112.016803 for a description of the full band structure of a thin EuO(111) film according to DFT calculations.
[25] E. Şaşıoğlu, C. Friedrich, and S. Blügel, Phys. Rev. Lett. **109**, 146401 (2012).
[26] D. E. Eastman, F. Holtzberg, and S. Methfessel, Phys. Rev. Lett. **23**, 226 (1969).
[27] D. F. Förster, Ph.D. thesis, Universität zu Köln, 2011.
[28] R. M. Feenstra and J. A. Stroscio, J. Vac. Sci. Technol. B **5**, 923 (1987).
[29] S. Modesti, H. Gutzmann, J. Wiebe, and R. Wiesendanger, Phys. Rev. B **80**, 125326 (2009).
[30] L. Petersen and P. Hedegård, Surf. Sci. **459**, 49 (2000).
[31] N. J. C. Ingle and I. S. Elfimov, Phys. Rev. B **77**, 121202 (2008).
[32] T. König, G. H. Simon, H.-P. Rust, and M. Heyde, J. Phys. Chem. C **113**, 11301 (2009).